

# A new high-resolution model for India–Capricorn motion since 20 Ma: Implications for the chronology and magnitude of distributed crustal deformation in the Central Indian Basin

C. DeMets\* and J.-Y. Royer<sup>†</sup>

Geology and Geophysics, University of Wisconsin-Madison, Madison, WI 53706, USA

<sup>†</sup>UBO-IUEM Domaines Oceaniques, Brest, France

We use more than 5000 crossings of magnetic anomalies and fracture zones along the Carlsberg and Central Indian ridges to examine whether the onset of widespread reverse faulting at ~8 Ma in the Central Indian Basin was accompanied by a significant change in India–Capricorn motion, whether the onset of this faulting represented the initiation of motion between these two plates, and whether the predicted shortening since 8 Ma agrees within uncertainties with fault-related shortening estimated from marine seismic profiles. The new high-resolution plate kinematic model, which specifies India–Capricorn finite and stage rotations at 20 distinct ages since 20 Ma, predicts that motion across the equatorial Indian Ocean was extremely slow from 17.4 Ma to 8 Ma, averaging less than 1 mm yr<sup>-1</sup> everywhere along the plate boundary. A significant acceleration in the rate of angular rotation at 8 Ma ended the period of slow or possibly no motion and constitutes the first evidence for a significant change in India–Capricorn plate motion at this time. The change in motion at ~8 Ma coincided remarkably well with the onset of widespread reverse faulting in the Central Indian Basin, suggesting a cause–effect relationship. Despite evidence for the period of nearly negligible motion from 17.4 Ma to 8 Ma, motion of ~1–2 mm yr<sup>-1</sup> from 20.1 Ma to 17.4 Ma (chrons 6no-5D) is highly significant, thereby implying that the onset of faulting at ~8 Ma did not mark the time that India–Capricorn motion began. The total north-to-south shortening predicted by the 7.9 Ma finite rotation agrees within uncertainties with shortening estimated from faults imaged along marine seismic profiles, thereby indicating that most or all shortening of the upper crust since 8 Ma has been accommodated by faulting.

PLATE kinematic data from the Carlsberg and Central Indian ridges were first used more than a decade ago<sup>1</sup> to demonstrate that the broad zone of actively deforming lithosphere south of India represents a wide boundary between the Indian and Australian plates (Figure 1). Subsequent progress in improving our understanding of this

once-enigmatic deforming region has occurred on two fronts. Analyses of magnetic lineations and oceanic fracture zones from the Central Indian and Carlsberg ridges have been used to construct increasingly precise models of motion across the deforming zone<sup>2–7</sup>. Independent of this work, marine seismic profiles and sediment cores have been used to establish the stratigraphic relations and ages for seismic unconformities that record episodes of wide spreading faulting within the deforming zone<sup>8–13</sup>, the earliest of which occurred at ~7.5 Ma. Marine seismic transects of the deforming zone further indicate that the cumulative shortening accommodated by this faulting decreases from east-to-west<sup>14–16</sup>, in accord with the predictions of plate kinematic models.

Although published plate kinematic models now successfully describe the observed patterns of deformation and

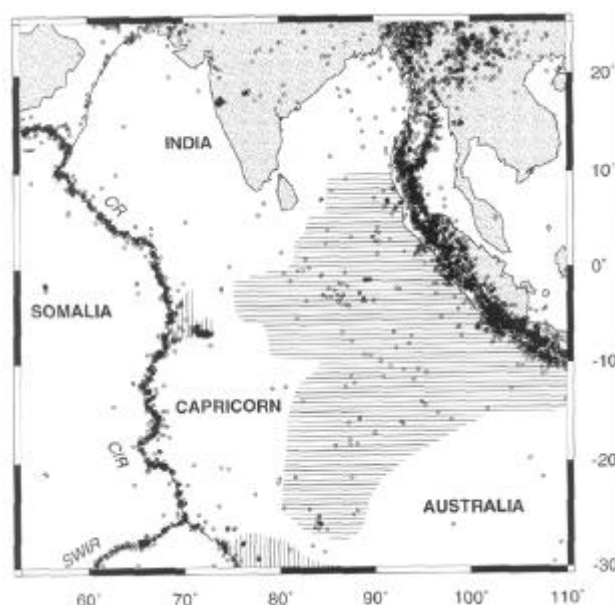


**Figure 1.** Location map and plate geometry adopted for this study. Small solid circles show the locations of 1963–2000 earthquakes of all magnitudes above depths of 60 km. Vertically striped regions are diffuse plate boundaries across which divergence is accommodated; the horizontally striped regions show diffuse plate boundaries across which convergence is accommodated. CR, Carlsberg Ridge; CIR, Central Indian Ridge; SWIR, Southwest Indian Ridge.

\*For correspondence. (e-mail: chuck@geology.wisc.edu)

provide useful estimates of strain and strain-rates across the deforming zones that separate the Indian and Capricorn plates, they lack the requisite temporal resolution to treat the following important questions: (1) Was the onset of widespread reverse faulting in the central Indian basin at  $\sim 7.5$  Ma accompanied by a significant change in India–Capricorn motion? (2) Does the onset of this faulting mark the initiation of motion between distinct Indian and Capricorn plates? (3) Do estimates of fault-related shortening since 8 Ma from marine seismic transects of the plate boundary agree with shortening predicted by the India–Capricorn finite rotation for C4n.2 (chron 4n.2), which describes motion since 7.86 Ma?

In another paper<sup>17</sup>, we use 2727 airborne and shipboard crossings of seafloor spreading magnetic lineation and 2545 satellite crossings of fracture zones flanking the Carlsberg and Central Indian ridges to derive India–Somalia and Capricorn–Somalia finite and stage rotations for 20 different ages since the beginning of C6. The data used to derive these rotations are displayed in Figure 2; further details regarding the data and procedures used to analyse them are given elsewhere<sup>17</sup>. The ages of the 20 magnetic anomalies we use are separated by intervals ranging from 0.7 Myr to 2.0 Myr, yielding a model for

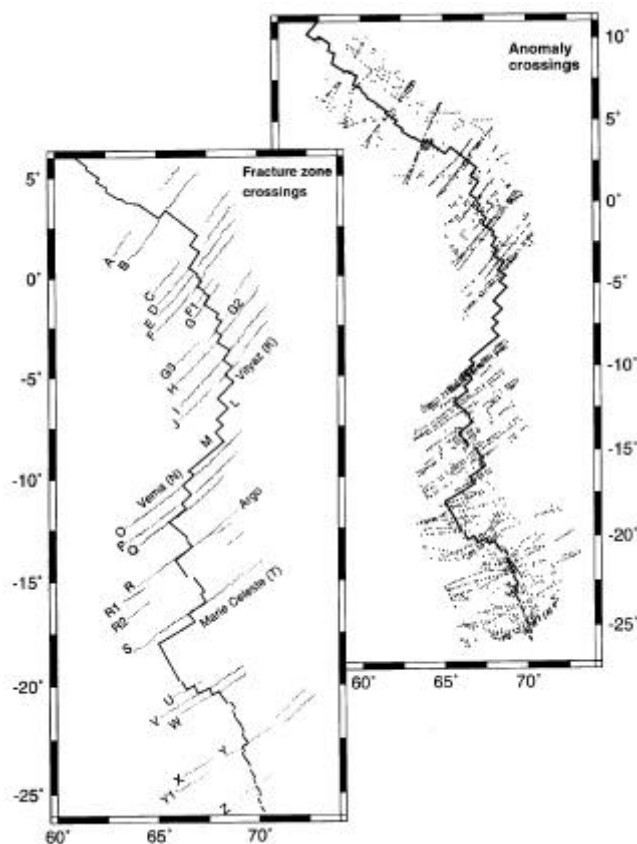


**Figure 2.** Locations of India–Somalia and Capricorn–Somalia magnetic anomaly crossings and fracture zone crossings used to derive India–Capricorn rotations. Further details regarding these data and their reconstructions are given by DeMets *et al.*<sup>17</sup>.

the motions of these plates of unprecedented temporal resolution. We find that India–Somalia and Capricorn–Somalia slip rates and slip directions changed significantly at  $\sim 9$  Ma to 8 Ma, approximately the time that faulting within the equatorial deforming zone began.

Herein, we construct an equally detailed model of India–Capricorn rotations from the same data and demonstrate that India–Capricorn motion also changed significantly at  $\sim 9$  Ma to 7 Ma. We further demonstrate that the data are fit nearly as well by a model in which the two plates are constrained to rotate about fixed stage poles during 20.1 Ma to 10.9 Ma and 7.9–0 Ma. We use the more precise, simpler models for India–Capricorn motion to demonstrate that motion changed significantly at  $\sim 8$  Ma, following a period of slow but non-zero motion from 17.4 Ma to 8 Ma. We conclude by showing that the new model predicts north-to-south shortening since 7.9 Ma that agrees within uncertainties with shortening estimated from marine seismic transects of the wide plate boundary east of 78°E.

### India–Capricorn kinematics: Best-fitting and fixed-pole models

The best-fitting India–Capricorn finite rotation for a given time (Table 1) is derived from the rotations that best reconstruct India–Somalia and Somalia–Capricorn anomaly and fracture zone crossings for that time<sup>17</sup>. We solve for the best-fitting rotations using well-established techniques<sup>18,19</sup> for reconstructing magnetic anomaly and fracture zone crossings from a paleo-spreading center. Uncertainties in the India–Somalia and Capricorn–Somalia rotations are determined rigorously from the uncertainties assigned to the individual magnetic anomaly and fracture zone crossings<sup>4</sup>. Uncertainties in the India–Capricorn rotations are then propagated from the India–Somalia and Capricorn–Somalia rotation covariances.

Figure 3 shows the best-fitting India–Capricorn poles for each of the 20 ages we selected. Given that the 20 poles are derived from independent sets of magnetic anomaly crossings and nearly independent sets of fracture zone crossings, the fact that the poles are strongly clustered is strong evidence that the underlying kinematic data usefully constrain India–Capricorn motion. Except for the loosely constrained poles for C1 and C2, the best-fitting India–Capricorn rotation poles are located from 73°E–78°E (Figure 3), in the aseismic portion of the plate boundary. The poles predict a transition from divergence west of  $\sim 75^\circ$ E to convergence to the east, in accord with results from prior studies<sup>1,3–7</sup>. Reconstruction of the displacement paths of three points located at the northern rigid edge of the Capricorn plate (points A, B, and C in the upper panel of Figure 3) using the best-fitting rotations yields a series of reconstructed positions that generally describe a small circle. To first order, India–Capricorn

**Table 1.** India–Capricorn total rotations and covariances

Chron	Lat (°N)	Long. (°E)	$\Omega$ (Degrees)	Covariances					
				<i>a</i>	<i>b</i>	<i>c</i>	<i>d</i>	<i>e</i>	<i>f</i>
1	10.62	86.83	0.252	317.3	438.2	-162.1	928.8	-117.4	170.3
2	1.28	78.73	0.563	618.1	896.6	-299.2	1868.1	-269.8	242.6
2An.1	-3.14	74.87	0.731	628.8	999.2	-263.3	2120.5	-250.8	221.6
2An.3	-1.47	76.24	0.983	634.9	1028.0	-257.0	2258.6	-258.7	206.4
3n.4	-6.79	73.08	1.393	206.3	2226.8	-442.2	4927.4	-515.7	345.5
3An.1	-3.14	73.98	1.960	1937.5	3767.6	-649.3	8893.3	-664.2	567.5
3An.2	-4.69	73.07	2.132	1674.0	2754.4	-823.0	5653.1	-926.4	662.8
4n.2	-4.76	73.31	2.556	1525.9	1986.9	-902.0	3805.4	-778.9	796.3
4A	-3.98	77.03	1.922	1584.3	2094.2	-884.1	4083.5	-753.3	825.1
5n.1	-7.45	74.84	2.292	1858.1	3248.5	-787.3	7028.1	-1053.9	629.4
5n.2o	-4.14	74.49	2.618	1222.6	1744.7	-623.3	3852.8	-681.0	526.0
5An.2	-4.89	73.59	2.769	1022.2	1781.0	-351.8	4247.1	-426.9	370.0
5AD	-2.91	74.36	2.781	1888.5	3880.9	-855.4	9160.6	-1593.3	673.2
5Bn.2	-3.93	76.50	2.394	2373.4	5118.9	-1003.0	12235.5	-2074.9	825.7
5Cn.1	-4.90	73.10	3.273	1635.9	3624.9	-487.1	8971.7	-776.4	496.6
5Cn.3	-5.23	75.00	2.901	895.5	1762.0	-314.9	4212.4	-481.8	310.0
5D	-4.32	74.68	2.881	1315.8	2522.1	-566.1	6007.3	-932.7	433.3
5E	-4.35	75.44	3.180	1089.4	2204.3	-402.4	5390.7	-695.8	287.3
6ny	-3.28	75.54	3.244	2426.6	5044.3	-782.5	12072.0	1313.2	612.0
6no	-3.19	75.33	3.434	1488.3	2839.5	-508.6	6790.3	-750.6	435.7

Rotations are derived in a fixed India reference frame. Covariances are Cartesian and have units of  $10^{-8}$  radians<sup>2</sup>. Elements *a*, *d* and *f* are the variances of the (0°N, 0°E), (0°N, 90°E), and 90°N components of the rotation. The covariance matrices are reconstructed as follows:

$$\begin{pmatrix} a & b & c \\ b & d & e \\ c & e & f \end{pmatrix}$$

motion has thus followed a relatively steady trajectory since 20 Ma.

Given that the India–Capricorn rotation poles for most times are located within each other’s confidence regions, we tested whether the anomaly and fracture zone crossings could be fit nearly as well if we employed a simpler model for India–Capricorn motion, one in which the pole of rotation and possibly the angular rotation rate remain fixed for long periods. Because such a model consists of many fewer rotation parameters than does a model that employs a distinct best-fitting rotation for each age (Table 1), it has the potential to describe India–Capricorn motion more accurately and precisely than does a best-fitting model (Table 1).

Based on results presented in our related analysis of India–Somalia and Capricorn–Somalia anomaly and fracture zone crossings<sup>17</sup>, we tested the fit of a kinematic model that assumes motion was steady during two extended intervals since 20 Ma, namely, from the present back to 7.9 Ma (C4n.2) and from 10.9 Ma (C5n.2o) back to 20.1 Ma (C6no). For both intervals, we first tested whether the data are consistent with motion about a stationary rotation pole with a variable rate of angular rotation. We refer to this model as a ‘fixed-pole’ model. We then tested whether the data are additionally consistent with both a stationary rotation axis and constant rate of angular rotation during each interval. We refer to this model as a ‘constant-motion’ model. The fixed-pole model

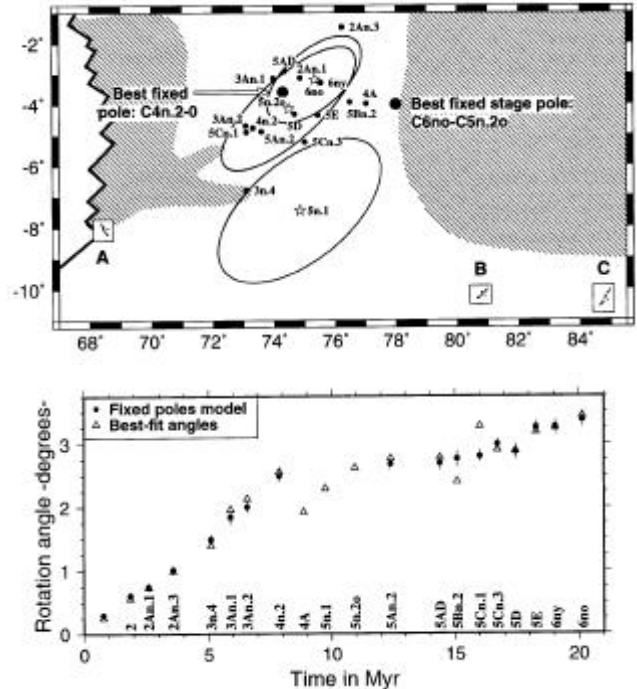


**Figure 3.** Upper, India–Capricorn best-fitting rotation poles, fixed poles, and selected 2-D 95% confidence regions (Table 1). Poles and confidence regions for C5n.1y, C5n.2o, and C6no are shown with open stars and bold lines. Insets A, B, and C are detailed in Figure 4. Lower, Time series of India–Capricorn rotation angles for best-fitting (open triangles) and fixed-poles (circles) models. Indian plate is fixed.

requires only one set of pole coordinates per interval and  $N$  rotation angles for  $N$  time steps, totaling  $2 + N$  rotation parameters per interval. The constant-motion model, representing the simplest possible description of motion through time, requires only three rotation parameters per interval – the pole coordinates and a constant angular rotation rate. In contrast, the best-fitting rotations employ different poles and rotation angles for each time, totalling  $3 \times N$  rotation parameters. The weighted least-squares fits ( $\chi^2$ ) of these models are compared using the  $\chi^2$  statistical test, which is appropriate since the data uncertainties are approximately correct.

We tested for motion about a stationary rotation axis by fixing the pole to the weighted mean location of the India–Capricorn finite rotations for C1–C4n.2 (3.6°S, 74.3°E) and solving for the opening angle for each chron that minimized the summed least-squares fit to the India–Somalia and Capricorn–Somalia anomaly and fracture crossings for that chron. Repeating this procedure for each of the eight chrons from C1 to C4n.2 yields a time series of eight opening angles (lower panel of Figure 3) that optimize the fit to the data subject to the assumption of a fixed pole during this interval. Fitting the 1616 India–Somalia data and 874 Capricorn–Somalia data for C1–C4n.2 in this manner yielded  $\chi^2 = 1220.5$  for the fixed-pole model and  $\chi^2 = 1198.9$  for the best-fitting rotations (Table 1). India–Capricorn rotations consist of three parameters for each of C1–C4n.2 (24 parameters) whereas the fixed-pole rotations consist only of the two fixed-pole coordinates and eight adjustable rotation angles. The difference in the least-squares fits of the fixed-pole and best-fitting models is thus a consequence of the 14 additional parameters that are employed by the latter model to fit the data. The difference in the least-squares fits of the two models,  $\Delta\chi^2 = 21.6$ , is significant at only the 91% confidence level, indicating the data are consistent with a stationary axis of rotation during this period. A similar test for a fixed pole of rotation extending back to 8.9 Ma (C4A) failed at the 99% confidence level.

Given that the data are well fit by a model that assumes a stationary rotation axis for the present back to C4n.2, we further tested whether the eight opening angles determined using the fixed pole are consistent with a constant angular rotation rate. Linear regression of the eight fixed-pole rotation angles for C1–C4n.2 (Figure 3) using magnetic anomaly reversal ages<sup>20</sup> and allowing for reversal age uncertainties of  $\pm 0.01$  Myr yields a best-fitting angular rotation rate and intercept of  $0.301^\circ/\text{Myr} \pm 0.01^\circ/\text{Myr}$  (1- $\sigma$ ) and  $0.02 \pm 0.04^\circ$ , with  $\chi^2$  of 5.1. Similarly, regression of the rotation angles using astronomically-tuned reversal ages<sup>21</sup> gives a best slope and intercept of  $0.297^\circ/\text{Myr} \pm 0.01^\circ/\text{Myr}$  and  $0.03^\circ \pm 0.04^\circ$ , with  $\chi^2$  of 4.8. Both values of reduced chi-square are less than 1.0, indicating that the fixed-pole opening angles are consistent with a constant angular rotation rate no matter which set of magnetic reversal ages we employ. The data are

thus consistent with steady India–Capricorn motion from 7.9 Ma to the present.

We also repeated the fixed-pole test for C6no–C5n.2o (20.1 Ma to 10.9 Ma). A grid search for the best stationary interval pole and ten associated rotation angles for C6no–C5n.2o yields a pole located at 4°S, 78°E (Figure 3). Although the difference in the least-squares fits of the fixed-pole and best-fitting models is significant at the 98% confidence level, the variance (e.g. summed least-squares misfit) for the simpler fixed-stage-pole model is only 4% larger than that for the latter model. There is thus only a small penalty in the fit associated with a fixed-pole model for India–Capricorn motion from C6no to C5n.2o.

The time series of rotation angles for the C6no–C5n.2o fixed-pole model (lower panel of Figure 3) exhibits significantly less scatter than do the best-fitting rotation angles, particularly for C5Bn.2 and C5Cn.1. Linear regression of the fixed-pole rotation angles for C6no–C5n.2o using Cande and Kent's<sup>20</sup> reversal ages yields a best-fitting angular rotation rate of  $0.100^\circ/\text{Myr} \pm 0.015^\circ/\text{Myr}$ , with  $\chi^2 = 8.4$ . Reduced chi-square for the linear fit is 1.05, indicating that the rotation angles are consistent with a constant angular rotation rate from 20.1 Ma to 10.9 Ma.

The time-progression of rotation angles for the fixed-stage-pole model (lower panel, Figure 3) strongly confirms the pattern defined by the noisier best-fitting rotation angles, namely, that India–Capricorn motion accelerated significantly between C4A and C4n.2 (8.9 Ma and 7.9 Ma). Interval rates along flow lines A and C (lower panel, Figure 4) determined from the fixed poles and best fixed-pole angles (upper panel, Figure 3) exhibit the acceleration in India–Capricorn motion implied by the factor-of-three increase in the angular rotation rate for 7.9–0 Ma versus 20.1 Ma to 10.9 Ma. From 15 Ma to 7.9 Ma, rates everywhere along the plate boundary averaged  $\sim 0\text{--}1$  mm  $\text{yr}^{-1}$ . After 7.9 Ma, rates accelerated to  $3\text{--}4$  mm  $\text{yr}^{-1}$  of divergence along flow line A and  $6\text{--}7$  mm  $\text{yr}^{-1}$  of convergence along flow line C (Figure 4). The simpler kinematic model thus confirms the speed up in India–Capricorn motion at  $\sim 8$  Ma that is suggested by the noisier best-fitting rotations.

### Evidence for periods of slow or no motion

Very slow interval rates before  $\sim 8$  Ma (Figure 4) suggest that India–Capricorn motion might not have started until  $\sim 8$  Ma, possibly coinciding with the onset of widespread reverse faulting in the Central Indian Basin. Following the lead of Gordon *et al.*<sup>7</sup>, who use a subset of the data described above to demonstrate that significant India–Capricorn motion occurred from 20.1 Ma to 10.9 Ma (C6no–C5n.2o), we repeat a test for significant India–Capricorn motion before 8 Ma using the more numerous data now available.

We first test for significant motion from 20.1 Ma to 7.9 Ma by comparing the interval rotation for C6no–

C4n.2 to the null rotation. To do so, we use the quadratic form of the chi-square test  $\chi^2 = \bar{\Omega}^T C_{\Omega} \bar{\Omega}$ , where  $\bar{\Omega}$  is the  $3 \times 1$  Cartesian representation of the small-angle interval rotation and  $C_{\Omega}$  is a  $3 \times 3$  matrix that contains the Cartesian covariances of the interval rotation. Applying this to the C6no–C4n.2 rotation gives  $\chi^2 = 52.4$ . The probability that a null rotation perturbed by random errors would yield such a high value for  $\chi^2$  is only two parts in  $10^{11}$ . Motion during this period was thus highly significant, albeit slow. Applying the same test to interval rotations for the two oldest intervals in our model, 19.0 Ma to 17.4 Ma and 20.1 Ma to 18.3 Ma, suggests that significant motion occurred during both intervals, albeit at somewhat lower confidence levels (99.8%). This corroborates results reported elsewhere<sup>7</sup> for significant motion from 20.1 Ma to 18.3 Ma.

A variety of additional checks, described below, strongly suggest that the motion implied for 20.1 Ma to 7.9 Ma is not a statistical fluke. The India–Capricorn interval rotation for C6no–C4n.2 predicts slow north-to-south divergence at locations west of  $\sim 80^\circ\text{E}$  and slow north-to-south convergence at locations to the east, the same as, but much slower than the India–Capricorn total rotations for all

times younger than 7.9 Ma. Given that the pre-7.9 Ma interval rotation and the post-7.9 Ma rotations are derived from disjoint sets of anomaly and fracture zone crossings, it seems unlikely that both would predict similar motion if one were a statistical anomaly. Tests for significant motion from C6no–C4n.2 using alternative India–Capricorn interval rotations derived from India–Somalia rotations that exclude the potentially less reliable data from the Carlsberg Ridge northwest of fracture zone B also indicate that India–Capricorn motion occurred before C4n.2. Finally, we also considered but rejected the possibility that our application of uniform phase shifts to long airborne and shipboard profiles caused small biases in the locations of anomaly crossings, which in turn biased the India–Somalia and Capricorn–Somalia opening angles. Synthetic magnetic profiles we constructed to study this possibility suggest that any such biases are an order-of-magnitude smaller than the predicted India–Capricorn displacements, 15–30 km, for locations along the Carlsberg and Central Indian ridges from 20.1 Ma to 7.9 Ma.

Although the absence of evidence in marine seismic profiles for folding or reverse faulting<sup>13</sup> before 8 Ma could be construed as evidence that India–Capricorn motion did not begin until after 8 Ma, the fixed-pole and best-fitting India–Capricorn interval rotations for C6no–C4n.2 ( $4^\circ\text{S}$ ,  $78^\circ\text{E}$  and  $1.5^\circ\text{N}$ ,  $81.0^\circ\text{E}$ , respectively) are located several angular degrees to the northeast of the rotation poles that describe India–Capricorn since 8 Ma and thus predict minimal shortening along the seismic profiles examined elsewhere<sup>13</sup>. For example, the C6no–C4n.2 fixed-pole interval rotation predicts cumulative latitudinal shortening of only  $1 \pm 2$  km (95%),  $5 \pm 3$  km, and  $11 \pm 6$  km at the mid-points of marine seismic profiles<sup>20</sup> at  $78.8^\circ\text{E}$ ,  $81.5^\circ\text{E}$ , and  $84.5^\circ\text{E}$ . If the minor predicted shortening along these profiles was accommodated over a broad area, possibly including lithosphere north or south of the zone of presently active faulting and folding, it might have little or no expression in the seismic profiles<sup>13</sup>.

### Changes in India–Capricorn motion from 10.9 Ma to 7.9 Ma

An unattractive aspect of the India–Capricorn kinematic model described above is the apparent departure during 10.9 Ma to 7.9 Ma from the relative steady increases in crustal shortening that characterizes motion before 10.9 Ma and after 7.9 Ma. For example, the rotations for C4A and C5n.1 predict significantly less cumulative shortening (Figure 5) than does the rotation for C4n.2 (7.9 Ma) and several later times. This implies that divergence occurred across much of the India–Capricorn plate boundary from 10.9 Ma to 7.9 Ma, which seems unlikely. Did India–Capricorn motion depart from steady state shortening during a several million year period prior to 7.9 Ma or is the apparently unsteady motion prior to 7.9 Ma an arti-

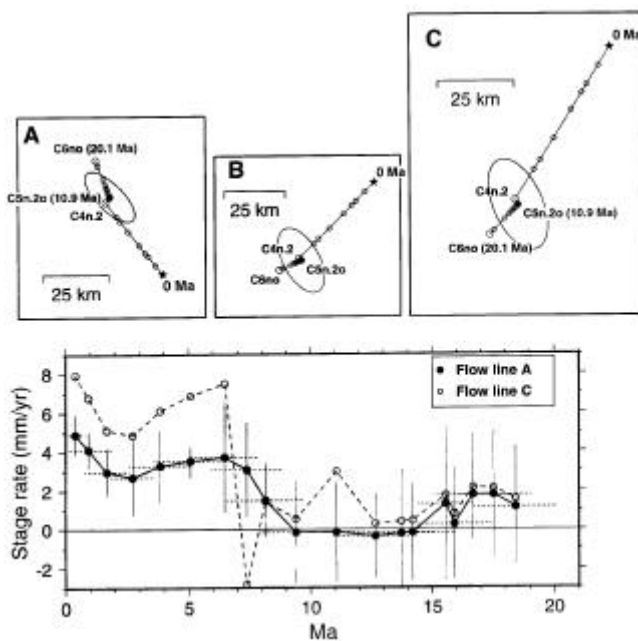


**Figure 4.** Panels A–C show flow lines for points A–C on the northern edge of the Capricorn plate (Figure 3) reconstructed relative to the Indian plate. Open circles are reconstructed using fixed-pole model described in text and filled circles are reconstructed using best-fitting rotations for C4A, C5n.1, and C5n.2o, for which no fixed-pole model exists. Uncertainty ellipse (2-D 95%) is shown for the reconstructed position of C5n.2o. Lower, India–Capricorn interval rates (circles) along flow lines A and C from upper panel. Interval rates are computed using the fixed-poles models for C1–C4n.2 and C5n.2o–C6no (upper panel) and the best-fitting rotations for C4A and C5n.1y. For clarity, rate uncertainties are omitted for flow line C, but average  $\pm 2$ – $3$  mm/yr. Reversal ages correspond to those assigned by Cande and Kent<sup>20</sup>. Dotted horizontal lines indicate the interval used to solve for a given rate. Uncertainties in all panels are  $1 \sigma$ . Indian plate is fixed.

fact of errors in our magnetic anomaly and fracture zone crossings for C4A and C5n.1?

We tested the latter hypothesis by examining whether one or both of the Capricorn–Somalia or India–Somalia rotations for C4A and C5n.1 are adversely affected by a mismatched spreading or fracture zone segment or by miscorrelated anomalies within a segment. Proceeding along the length of each plate boundary, we systematically deleted single segments of data, inverted the remaining data to solve for a best-fitting reconstruction, and examined the resulting fits and rotations. This did not significantly improve the fit or significantly change the locations of the alternative best-fitting rotations. We also inverted the C4A and C5n.1 India–Somalia data while eliminating all crossings of the sparsely sampled magnetic anomalies along the Carlsberg Ridge northwest of FZ B. This also had little effect. The data we employ for the northwestern half of the Carlsberg Ridge are thus consistent with the unambiguous and easily interpreted magnetic anomalies and fracture zones southwest of FZ B. These results, when coupled with the fact that the dispersions for the reconstructions for C4A and C5n.1 do not differ significantly from those for the other times, suggest that the unsteady India–Capricorn motion from 10.9 Ma to 7.9 Ma is not easily attributed to noise in the underlying data.

An alternative explanation may be that distributed deformation between the Indian and Capricorn plates extended significantly north of its present limit during times before 7.9 Ma. Such deformation could have affected

the paleo-opening rates and directions along the northern Central Indian Ridge, thereby introducing a systematic error into the India–Somalia magnetic anomaly and fracture zone crossings that we use to constrain the India–Capricorn rotations for these two times. More and better data from the Carlsberg Ridge northwest of FZ B are needed to further study this hypothesis.

### Comparison to marine seismic estimates of shortening

Estimates of post-8 Ma shortening across the equatorial deforming zone are available from three N–S marine seismic transects that image reverse faults in the convergent part of the India–Capricorn plate boundary. Transects located at 78.8°E and 81.5°E<sup>14,16</sup> span the entire deforming zone and a third, at 84.5°E<sup>15</sup>, crosses only part of the plate boundary and thus gives only a lower bound for the total shortening.

The latitudinal components of shortening predicted by the 7.9 Ma (C4n.2) rotation are consistent within uncertainties with estimates for the marine seismic transects at 81.5°E and 84.5°E (Figure 5), but significantly exceed the shortening estimated for the 78.8°E profile. Reverse faulting along two of the three seismic profiles thus appears to have accommodated most or all of the shortening predicted to have occurred following the onset of faulting at 8 Ma to 7.5 Ma. This agrees with evidence<sup>3,22</sup> that shortening accommodated by folding accounts for only a few kilometers or less of the total shortening budget.

### Discussion and conclusions

The results described above reveal or reinforce several interesting features of post-20 Ma India–Capricorn motion. The kinematic data for C1–C4n.2 are consistent with a constant rotation axis and constant angular rotation rate, indicating that India–Capricorn motion has been steady since 7.9 Ma. A significant acceleration of motion at 7.9 Ma ended an extended interval of slow motion from 17.4 Ma to 7.9 Ma and coincided with the initiation of widespread reverse faulting in the Central Indian Basin. The new kinematic model confirms evidence<sup>7</sup> for significant India–Capricorn motion from 20.1 Ma to 17.4 Ma. The search for the initiation of India–Capricorn motion must thus be extended to older times.

Both the best-fitting and fixed-pole models indicate that the acceleration in India–Capricorn motion (Figure 3) occurred no later than 7.9 Ma (C4n.2) and no earlier than 8.9 Ma (C4A). Its coincidence with the well-dated onset of widespread reverse faulting south of India clearly suggests a cause-and-effect relationship. We reject an alternative explanation for the acceleration, namely, that it is an indirect consequence of a possible change at 8 Ma

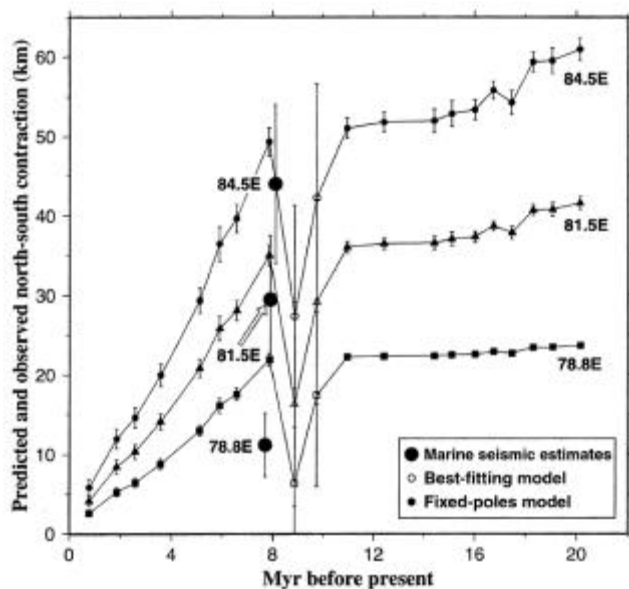


**Figure 5.** Predicted and observed latitudinal (N–S) components of India–Capricorn contraction since 20.1 Ma along marine seismic transects<sup>14–16</sup> at 78.8°E, 81.5°E, and 84.5°E. Large symbols show shortening and 95% uncertainty estimated from seismic profiles. Solid symbols depict shortening predicted by the fixed-poles model described in the text. Open symbols show N–S shortening predicted by best-fitting rotations for C4A and C5n.1 (Table 1). Model errors are 1  $\sigma$ . Indian plate is fixed.

in the absolute motion of the Somalia plate, because a change in the rotation of the Somalia plate relative to the underlying mantle would propagate equally into India–Somalia and Capricorn–Somalia rotations and would thus cancel.

Changes at or before ~ 8 Ma in the forces acting on the edges of the Indian or Capricorn plates are thus likely to be responsible for the observed changes in their motions. For example, the onset of extension within the Tibetan plateau at ~ 8 Ma, presumably in response to its gravitational collapse after attaining its maximum elevation, may have significantly changed the forces exerted along the northern edge of the Indian plate<sup>23–27</sup>. Alternatively, the observed onset of faulting at 8–7.5 Ma within the equatorial plate boundary separating the Indian and Capricorn plates may have altered the balance of forces along the India–Capricorn boundary, thereby explaining the simultaneous change in the motions of both plates with respect to one another and relative to Somalia. Ultimately, attempts to explain the cause of the changes at ~ 8 Ma in India–Somalia–Capricorn motions will require a reliable chronology of changes in the torques acting on all three plates and a better understanding of the mechanics of stress transfer across their shared boundaries.

1. Wiens, D. A. *et al.*, A diffuse plate boundary model for Indian Ocean tectonics. *Geophys. Res. Lett.*, 1985, **12**, 429–432.
2. DeMets, C., Gordon, R. G. and Argus, D. F., Intraplate deformation and closure of the Australia–Antarctica–Africa plate circuit. *J. Geophys. Res.*, 1988, **93**, 11,877–11,897.
3. Gordon, R. G., DeMets, C. and Argus, D. F., Kinematic constraints on distributed lithospheric deformation in the equatorial Indian Ocean from present motion between the Australian and Indian plates. *Tectonics*, 1990, **9**, 409–422.
4. Royer, J.-Y. and Chang, T., Evidence for relative motions between the Indian and Australian plates during the last 20 Myr from plate tectonic reconstructions: Implications for the deformation of the Indo-Australian plate. *J. Geophys. Res.*, 1991, **96**, 11,779–11,802.
5. DeMets, C., Gordon, R. G. and Vogt, P., Location of the Africa–Australia–India triple junction and motion between the Australian and Indian plates: Results from an aeromagnetic investigation of the Central Indian and Carlsberg ridges. *Geophys. J. Int.*, 1994, **119**, 893–930.
6. Royer, J.-Y., Gordon, R. G., DeMets, C. and Vogt, P. R., New limits on the motion between India and Australia since chron 5 (11 Ma) and implications for lithospheric deformation in the equatorial Indian Ocean. *Geophys. J. Int.*, 1997, **129**, 41–74.
7. Gordon, R. G., DeMets, C. and Royer, J. Y., Evidence for long-term diffuse deformation of the lithosphere of the equatorial Indian Ocean. *Nature*, 1998, **395**, 370–374.
8. Moore, D. G., Curray, J. R., Raitt, R. W. and Emmel, F. J., Stratigraphic–seismic section correlations and implications to Bengal Fan history. *Initial Rep. Deep Sea Drill. Proj.*, 1974, **22**, 403–412.
9. Weissel, J. K., Anderson, R. N. and Geller, C. A., Deformation of the Indo-Australian plate. *Nature*, 1980, **287**, 284–291.
10. Curray, J. R. and Munasinghe, T., Timing of intraplate deformation, northeastern Indian Ocean. *Earth Planet. Sci. Lett.*, 1989, **94**, 71–77.
11. Cochran, J. R., Himalayan uplift, sea level and the record of Bengal Fan sedimentation at the ODP leg 116 sites. *ODP volume 116* (eds Cochran, J. R. *et al.*), 1990, pp. 397–414.
12. Krishna, K. S., Ramana, M. V., Gopala Rao, D., Murthy, K. S. R., Malleswara Rao, M. M., Subrahmanyam, V. and Sarma, K. V. L. N. S., Periodic deformation of oceanic crust in the central Indian Ocean. *J. Geophys. Res.*, 1998, **103**, 17,859–17,875.
13. Krishna, K. S., Bull, J. M. and Scrutton, R. A., Evidence for multi-phase folding of the central Indian Ocean lithosphere. *Geology*, 2001, **29**, 715–718.
14. Chamot-Rooke, N., Jestin, F., de Voogd, B. and Ph'edre Working Group, Intraplate shortening in the central Indian Ocean determined from a 2100-km-long north–south deep seismic reflection profile. *Geology*, 1993, **21**, 1043–1046.
15. Jestin, F., Cin'ematique rigide et d'ormations dans la jonction triple Afar et dans le basin Indien Central, Th' ese de Doctorat, 1994, Universit'e Pierre et Marie Curie, Paris.
16. Van Orman, J., Cochran, J. R., Weissel, J. K. and Jestin, F., *Earth Planet. Sci. Lett.*, 1995, **133**, 35–46.
17. DeMets, C., Gordon, R. G. and Royer, J.-Y., A new high-resolution model for India–Capricorn–Somalia plate motion since 20 Ma: Implications for the chronology and magnitude of distributed seafloor deformation in the Central Indian Basin, in revision. *Geophys. J. Int.*, 2003.
18. Hellinger, S. J., The statistics of finite rotations in plate tectonics, unpublished Ph.D. thesis, 1979, Massachusetts Institute of Technology, pp. 172.
19. Chang, T., Estimating the relative rotation of two tectonic plates from boundary crossings. *J. Am. Stat. Assoc.*, 1988, **83**, 1178–1183.
20. Cande, S. C. and Kent, D. V., Revised calibration of the geomagnetic polarity timescale for the Late Cretaceous and Cenozoic. *J. Geophys. Res.*, 1995, **100**, 6093–6095.
21. Hilgen, F. J., Krijgsman, W., Langereis, C. G., Lourens, L. J., Santarelli, A. and Zachariasse, W. J., Extending the astronomical (polarity) time scale into the Miocene. *Earth Planet. Sci. Lett.*, 1995, **136**, 495–510.
22. Bull, J. M. and Scrutton, R. A., Seismic reflection images of intraplate deformation, Central Indian Ocean and their tectonic significance. *J. Geol. Soc. London*, 1992, **149**, 955–966.
23. Armijo, R., Tapponnier, P., Mercier, J. L. and Han, T. L., Quaternary extension in southern Tibet: Field observations and tectonic implications. *J. Geophys. Res.*, 1986, **91**, 13,803–13,872.
24. England, P. C. and Houseman, G. A., Extension during continental convergence, with application to the Tibetan Plateau. *J. Geophys. Res.*, 1989, **94**, 17,561–17,579.
25. Harrison, T. M., Copeland, P., Kidd, W. S. F. and Yin, A., Raising Tibet. *Science*, 1992, **255**, 1663–1670.
26. Molnar, P., England, P. and Martinod, Mantle dynamics, uplift of the Tibetan plateau and the Indian monsoon. *Rev. Geophys.*, 1993, **31**, 357–396.
27. Edwards, M. A. and Harrison, T. M., When did the roof collapse? Late Miocene north–south extension in the high Himalaya revealed by Th–Pb monazite dating of the Khula Kangri granite. *Geology*, 1997, **25**, 543–546.
28. Wessel, P. and Smith, W. H. F., Free software helps map and display data. *EOS Trans. Am. Geophys. Union*, 1991, **72**, 441–446.

ACKNOWLEDGEMENTS. This work was supported by grants from the US National Science Foundation, the French Centre National de la Recherche Scientifique (CNRS), the Plan National de T'el'ed'ection Spatiale, and the NSF/CNRS cooperative program. Figures were drafted using GMT software<sup>28</sup>.